The Aeronautical Journal (2023), **127**, pp. 627–650
doi:10.1017/aer.2022.72

REGULAR PAPER

Enhanced backstepping control for an unconventional quadrotor under external disturbances

A. Belmouhoub[1,*], S. Medjmadj[2], Y. Bouzid[3], S. H. Derrouaoui[3] and M. Guiatni[3]

[1]Materials and Electronic Systems Laboratory, University of Mohamed El Bachir El Ibrahimi, Bordj Bou Arreridj, Algeria, [2]Laboratory of Control University of Setif and University of Bordj Bou Arreridj, Algeria and [3]Complex Systems Control and Simulators (CSCS) laboratory, Ecole Militaire Polytechnique, Bordj el Bahri, Algiers, Algeria
*Corresponding author. Email: belmouhoub.amina@gmail.com

Received: 25 November 2021; **Revised:** 21 June 2022; **Accepted:** 21 June 2022

Keywords: Unconventional quadrotor; Foldable drone; Backstepping control; Super-Twisting algorithm; Robust control.

Abstract

Robust control of non-linear systems is a challenging task, notably in the presence of external disturbances and uncertain parameters. The main focus of this paper is to solve the trajectory tracking problem of an unconventional quadrotor with rotating arms (also known as a foldable drone), while overcoming some of the challenges associated with this type of vehicle. Therefore, in a first step, the model of this vehicle is presented, taking into account the change of the inertia, the centre of gravity, and the control matrix. The theoretical foundations of backstepping control, based on the finite time Lyapunov stability theory and enhanced by a Super-Twisting algorithm, are then discussed. Numerical simulations are performed to demonstrate the efficiency of the suggested control approach. Finally, a qualitative and quantitative comparative study of the proposed controller with the conventional backstepping controller is performed. Overall, the obtained results show that the proposed control strategy outperforms in terms of accuracy and resilience.

Nomenclature

UAVs	Unconventional Unmanned Aerial Vehicles
PID	Proportional Integral Derivative
LQR	Linear Quadratic Regulator
ADRC	Active Disturbance Rejection Controller
SUAV	Subminiature UAV
MPC	Model Predictive Control
MRAC	Model Reference Adaptive Control
CoG	Center of Gravity
ST	Super Twisting

1.0 Introduction

Automation and robotisation in the aeronautical field are opening up new perspectives in terms of rescue, observation, inspection and reconnaissance [1, 2, 3]. Research in this field has been very active recently, and this growing interest is due to technological advances, particularly in the field of miniaturisation of actuators and onboard electronics.

Unconventional Unmanned Aerial Vehicles (UAVs) (called reconfigurable UAVs) are a new class of drones. They have a variable structure during flight. In recent years, they have gained great popularity and have been the subject of scientific researchers, and this is due to their ability to change their morphologies

to different flight conditions [4] and optimise their shape to achieve multitask missions [5, 6]. Changing the configuration during flight enables critical tasks that are difficult to complete with conventional quadrotors.

Unconventional UAVs are reliable in enclosed areas and dangerous places [7]. Infrastructure inspection and cave discoveries also require this type of vehicle [8, 9]. Furthermore, the ability to grasp and transfer large objects without the use of extra mechanisms and with minimum energy use is a significant advantage [10, 11]. Another key element is that modifying the configuration allows new movements like roll, pitch, yaw, and translation to be introduced without impacting the motors' rotation velocities [12]. Different structures have already been proposed by introducing changes to the classic drone such as the length and the number of arms [13, 14], control of the orientation of propellers and rotors, and other structures [15, 16].

Since the UAV is exposed to an unfavorable atmospheric environment and external conditions, reliable and robust control algorithms are required. In the literature, a large number of publications on multi-copters address this control problem. There are several control laws based on the linearisation of the dynamic model [17], although these approaches have limitations when the system moves away from its operating point. Some studies propose the development of linear controllers such as Proportional Integral Derivative (PID) and Linear Quadratic Regulator (LQR) [18, 19], while others suggest the development of non-linear methods to maintain the stability of the system [20, 21]. In Ref. [22], Gao et al. design an Active Disturbance Rejection Controller (ADRC), which is developed from the non-linear PID controller and applied to an unconventional Subminiature UAV (SUAV) system. Authors in Ref. [23] implement a linearisation control law based on the input-output feedback. The proposed control aims to stabilise both the tilt-rotor aircraft and the load over the entire trajectory. Another controller, Model Predictive Control (MPC), was presented by Richard et al. in reference [24] to solve the trajectory tracking problem of a linearised titled rotor drone when carrying a suspended load. Research [25] shows a controller based on state-dependent LQR for the high-level and a PID control for the low-level tilt-rotor. In the work of Desbiez et al. [5], a Model Reference Adaptive Control (MRAC) and a PID that controls the attitude have been applied to a multirotor with two independent rotating arms. The MRAC law has been used to manage the uncertainties due to the variable architecture of the quadrotors. In Ref. [26], Wallace et al. opted for a controller based on a LQR to stabilise the entire model of the folding arm drone initially, and then control the vehicle in a trirotor configuration in which the vehicle can transform. This controller is supposed to provide stability to the vehicle, but it did not generate consistent returns to the origin. Barbaraci et al. [27] also discussed the control algorithm using a LQR on a quadrotor with variable arm geometry, to stabilise the UAV and recover the error with respect to the reference, but in their case, they implemented the controller after linearising the system. Another study was made by Falanga et al. [28] to ensure stable flight at all times with any morphology transition, in which they exploit an adaptive LQR controller that adapts to the drone's morphology during the flight. A new and first design of a self-foldable and self-deployable drone is proposed by Tuna et al. [29], where the arms are rotated at the same time by a single servomotor. Recently, optimising energy consumption during flight has become an area of interest for Xiong. To ensure a best energy efficiency, they have proposed the rotation of the quadrotor's arms, to achieve the desired movements, while keeping the same thrust for each rotor. In Ref. [30], authors proposed a new set of morphing wings for drones, these wings provide an energy-efficient method of roll control.

The studied system in this paper is highly non-linear and has a variable structure during flight, which makes the control of this type of vehicle difficult and complex. Recent work has focused on conventional controllers for unconventional drones. The majority of the existing literature focuses on classical backstepping. However, this control law does not guarantee stability in the presence of uncertain parameters and unknown disturbances.

In this paper and following our previous work [4], we are interested in a nonlinear robust controller to ensure better tracking of a drone with rotating arms in the presence of unknown disturbances, taking

https://doi.org/10.1017/aer.2022.72 Published online by Cambridge University Press

into account the change of its Center of Gravity (CoG), the variation of the inertia, and the allocation matrix. The backstepping controller is used in combination with the Super-Twisting (ST) algorithm. The control law of ST is composed of two parts: the first one represents a convergence term, while the second one is a disturbance estimation term.

The main contributions of this work are summarised as follows:

- An enhanced backstepping controller with a correction term based on the ST algorithm is proposed. It has the particularity of solving the trajectory tracking problem in finite time and ensures quicker convergence, better performance, high accuracy, and robustness against disturbances.
- Tests are performed to demonstrate the performance of the developed controller. They are made under disturbances.
- A quantitative and qualitative comparative study involving our control strategy with a classical backstepping controller is provided to highlight the performance of our method.

The remainder of the paper is structured as follows: In Section II, a brief modeling of the unconventional quadrotor using the Newton-Euler formalism is presented, while in Section III the proposed non-linear control based on the hierarchical robust finite-time control approach and backstepping method is designed and applied to the studied quadrotor. In Section IV, the numerical simulation results are carried out. Finally, some concluding remarks are drawn.

Notation

The following notations will be used throughout this document:

Let $\mathbb{R}$ and $\mathbb{R}_+$ denote the set of real and positive real numbers respectively.

$\mathfrak{Sig}^{\beta}(r) = \left[|r_1|^{\beta}\text{sign}(r_1) \quad |r_2|^{\beta}\text{sign}(r_2) \quad |r_3|^{\beta}\text{sign}(r_3)\right]^T$, $\mathfrak{Int}(r) = \left[\int \text{sign}(r_1) \quad \int \text{sign}(r_2) \quad \int \text{sign}(r_3)\right]^T$, $r = \begin{bmatrix} r_1 & r_2 & r_3 \end{bmatrix}^T$, where $\text{sign}(\Theta) = \dfrac{\Theta}{|\Theta|}$ is the standard signum function and $|\Theta|$ refers to the absolute value of Θ. The notation $\|r\|$ refers to the Euclidean norm of vector r. The symbol $\wedge$ denotes the cross product. For the symmetric matrix $P \in \mathbb{R}^{n\times n}$, $\delta_{min}(P)$ and $\delta_{max}(P)$ are its minimum and maximum eigenvalues, respectively. $\text{diag}(a_1, a_2, \ldots, a_n)$ denotes the corresponding diagonal matrix. The notations $c(.)$ and $s(.)$ symbolise the functions cos(.) and sin(.), respectively.

2.0 Geometric description and modeling of the unconventional quadrotor

This section briefly presents the geometric description of the rotating arm drone and discusses its modeling.

2.1 Dynamic model of the disturbed attitude and translation of the unconventional quadrotor

The foldable drone can change the angles $\sigma_i(t)|_{i=1,\ldots,4}$ between its arms via the servomotors, these latter are linked to a central body as shown in Fig. 1. Each arm contains a rotor placed at its extremity. Changing the angular velocity of the rotors $\omega_i(t)|_{i=1,\ldots,4}$ and rotating the arms can change the shape of the foldable drone and produce other more complex configurations from the basic X configuration.

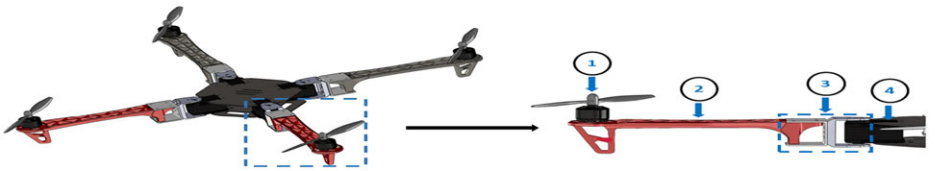

Figure 1. *Design of the quadrotor with rotating arms. (1) Propeller. (2) Rotating arm. (3) Servo-arm junction. (4) Servomotor.*

https://doi.org/10.1017/aer.2022.72 Published online by Cambridge University Press

In this paper, we have chosen six different configurations of the quadrotor with rotating arms in this order (X, Y, YI, H, T, O) as shown in Fig. 2 and Table 1.

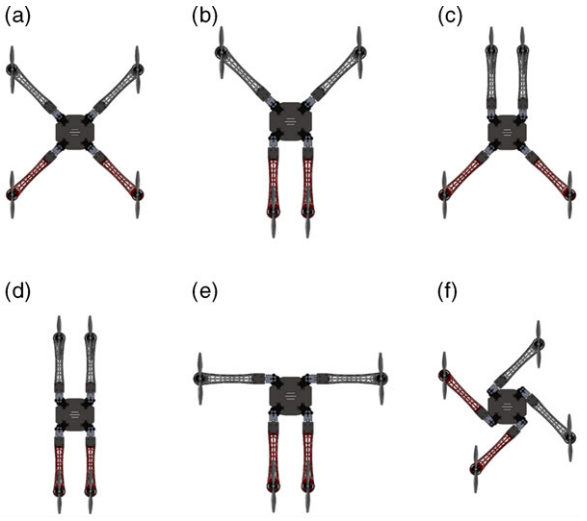

Figure 2. *Different configurations of the quadrotor with rotating arms: (a) X configuration, (b) Y configuration, (c) YI configuration, (d) H configuration, (e) T configuration, (f) O configuration.*

Table 1. *The arm angles of each configuration*

Configurations	Arm angles
X	$\sigma_1(t) = \pi/4, \sigma_2(t) = \pi/4, \sigma_3(t) = \pi/4, \sigma_4(t) = \pi/4$
Y	$\sigma_1(t) = \pi/4, \sigma_2(t) = \pi/4, \sigma_3(t) = \pi/2, \sigma_4(t) = 0$
YI	$\sigma_1(t) = \pi/2, \sigma_2(t) = 0, \sigma_3(t) = \pi/4, \sigma_4(t) = \pi/4$
H	$\sigma_1(t) = \pi/2, \sigma_2(t) = 0, \sigma_3(t) = \pi/2, \sigma_4(t) = 0$
T	$\sigma_1(t) = 0, \sigma_2(t) = \pi/2, \sigma_3(t) = \pi/2, \sigma_4(t) = 0$
0	$\sigma_1(t) = \pi, \sigma_2(t) = \pi, \sigma_3(t) = \pi, \sigma_4(t) = \pi$

The quadrotor with rotating arms is considered as a rigid body of which its motion in space can be represented by two coordinate frames: $B = (o, x_m, y_m, z_m)$ is the body-fixed frame attached to the centre of gravity of the aerial vehicle and $E = (o_i, x_i, y_i, z_i)$ is the earth-fixed frame as shown in Fig. 3.

Hypothesis

The following basic hypothesis are considered in quadrotor with rotating arms modeling:

- The quadrotor is a rigid body whose mass is constant.
- The propellers are rigid.
- The transition from one configuration to another is long so as not to generate abrupt phenomena.
- The angle of manoeuverability of the arms is assumed to be small.
- The rotation velocities of the arms are not too high.

https://doi.org/10.1017/aer.2022.72 Published online by Cambridge University Press

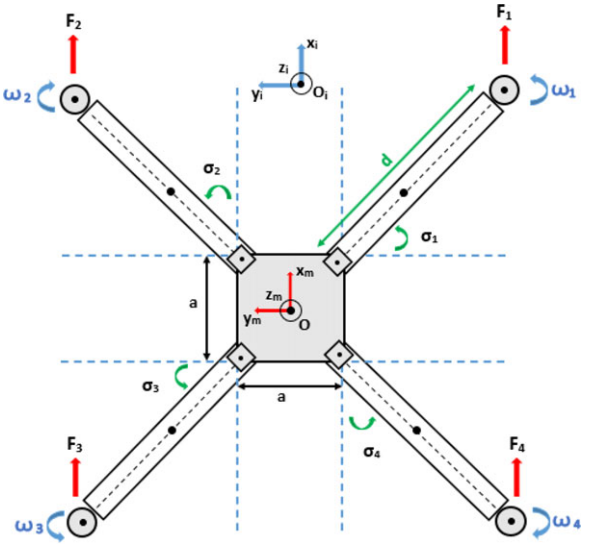

Figure 3. *Schematic of the quadrotor with rotating arms.*

We elaborate the dynamic equations of the system by using the Newton-Euler formalism. The system can be written in the following form [4]:

$$\begin{cases} \dot{\xi} = V \\ m\ddot{\xi} = R_\eta (F_t - F_g) + F_d + F_{ext} \\ \dot{R}_\eta = R_\eta \, Sk(\Omega) \\ J(\sigma(t))\dot{\Omega} = -Sk(\Omega) J(\sigma(t))\Omega + \Gamma_f - \Gamma_a - \Gamma_{gy} + \Gamma_{ext} \end{cases}, \tag{1}$$

where $\xi \in \mathbb{R}^3$ and $V \in \mathbb{R}^3$ are respectively the position and velocity of the quadrotor with rotating arms. m is the total mass of the quadrotor, which is supposed to be constant and $\Omega \in \mathbb{R}^3$ its angular velocity expressed in the body frame.

F_t, F_g and F_d belong to $\mathbb{R}^3$ are respectively the total force generated by the four rotors, the gravity force along the z-axis and the drag force along the three axes (x,y,z).

$$F_t = R \begin{bmatrix} 0 & 0 & \sum_{i=1}^{4} F_i \end{bmatrix}^T, \tag{2}$$

where

$$F_i = b \, w_i^2, \tag{3}$$

$$F_g = \begin{bmatrix} 0 & 0 & -mg \end{bmatrix}^T, \tag{4}$$

$$F_d = -\text{diag} \begin{pmatrix} K_{dfx} & K_{dfy} & K_{dfz} \end{pmatrix} \dot{\xi}, \tag{5}$$

with b is the aerodynamic coefficients and $K_{df(x,y,z)}$ are the translation drag coefficients.

$F_{ext} \in \mathbb{R}^3$ represents the disturbances according to the translation movement.

https://doi.org/10.1017/aer.2022.72 Published online by Cambridge University Press

Γ_f, Γ_{gy} and Γ_a belong to $\mathbb{R}^3$ are the moment caused by the thrust and drag forces, the gyroscopic torque of the propellers and the moment resulting from aerodynamic friction.

$$\Gamma_f = \begin{bmatrix} \Gamma_x & \Gamma_y & \Gamma_z \end{bmatrix}^T, \tag{6}$$

$$\Gamma_{gy} = \sum_{i=1}^{4} \Omega \wedge J_r \begin{bmatrix} 0 & 0 & (-1)^{i+1} w_i \end{bmatrix}^T, \tag{7}$$

J_r is the rotor inertia

$$\Gamma_a = \text{diag} \begin{pmatrix} K_{afx} & K_{afy} & K_{afz} \end{pmatrix}^T \Omega^2, \tag{8}$$

$\Gamma_{ext} \in \mathbb{R}^3$ is the disturbances according to the rotation movement.

$R_\eta \in \mathbb{R}^{3\times3}$ is the rotation matrix connecting the two frames of reference, it can be parameterised by Euler angles $\eta = (\phi, \theta, \psi)$:

$$R_\eta = \begin{bmatrix} c\psi c\theta & s\phi s\theta c\psi - s\psi c\phi & c\phi s\theta c\psi + s\psi s\phi \\ s\psi c\theta & s\phi s\theta s\psi + c\psi c\phi & c\phi s\theta s\psi - s\phi c\psi \\ -s\theta & s\phi c\theta & c\phi c\theta \end{bmatrix}, \tag{9}$$

$Sk \in \mathbb{R}^{3\times3}$ is the skew-symmetric matrix related to the angular velocity Ω

$$Sk = \begin{bmatrix} 0 & -r & q \\ r & 0 & -p \\ -q & p & 0 \end{bmatrix}. \tag{10}$$

The reconfiguration of the quadrotor, during the flight, generates a displacement of its CoG, a change of its inertia $J_{3\times3}(\sigma(t))$ and requires a readjustment of the allocation matrix. The calculation of the inertia matrix is mainly based on the theorem of Huygens-Steiner, the analytical details of calculation is presented in the works of Derrouaoui et al. [31, 32], in which some approximations are made to simplify the development.

2.2 Developed model

Dynamic model (1) can be written in terms of position, rotation and input as follow:

$$\begin{cases} \ddot{\phi} = f_\phi(t) + g_\phi(t) U_2 \\ \ddot{\theta} = f_\theta(t) + g_\theta(t) U_3 \\ \ddot{\psi} = f_\psi(t) + g_\psi(t) U_4 \\ \ddot{x} = f_x(t) + g_x(t) U_x U_1 \\ \ddot{y} = f_y(t) + g_y(t) U_y U_1 \\ \dot{z} = f_z(t) + g_z(t) U_1 \end{cases}, \tag{11}$$

https://doi.org/10.1017/aer.2022.72 Published online by Cambridge University Press

with

$$\begin{cases} f_\phi(t) = \dfrac{J_{yy}(\sigma(t)) - J_{zz}(\sigma(t))}{J_{xx}(\sigma(t))}\dot{\theta}\dot{\psi} - \dfrac{J_r\,\omega_r}{J_{xx}(\sigma(t))}\dot{\theta} - \dfrac{K_{afx}}{J_{xx}(\sigma(t))}\dot{\phi}^2 \\ g_\phi(t) = \dfrac{1}{J_{xx}(\sigma(t))} \\ f_\theta(t) = \dfrac{J_{zz}(\sigma(t)) - J_{xx}(\sigma(t))}{J_{yy}(\sigma(t))}\dot{\phi}\dot{\psi} + \dfrac{J_r\,\omega_r}{J_{yy}(\sigma(t))}\dot{\phi} - \dfrac{K_{afy}}{J_{yy}(\sigma(t))}\dot{\theta}^2 \\ g_\theta(t) = \dfrac{1}{J_{yy}(\sigma(t))} \\ f_\psi(t) = \dfrac{J_{xx}(\sigma(t)) - J_{yy}(\sigma(t))}{J_{zz}(\sigma(t))}\dot{\phi}\dot{\theta} - \dfrac{K_{afz}}{J_{zz}(\sigma(t))}\dot{\psi}^2 \\ g_\psi(t) = \dfrac{1}{J_{zz}(\sigma(t))} \\ f_x(t) = -\dfrac{K_{dfx}}{m}\dot{x} \\ g_x(t) = \dfrac{1}{m} \\ f_y(t) = -\dfrac{K_{dfy}}{m}\dot{y} \\ g_y(t) = \dfrac{1}{m} \\ f_z(t) = -\dfrac{K_{dfz}}{m}\dot{z} - g \\ g_z(t) = \dfrac{\cos\phi\,\cos\theta}{m} \end{cases}, \tag{12}$$

and

$$\begin{cases} U_x = (c\phi s\theta c\psi + s\phi s\psi) \\ U_y = (c\phi s\theta s\psi - s\phi c\psi) \\ \omega_r = \omega_1 - \omega_2 + \omega_3 - \omega_4 \end{cases}. \tag{13}$$

The model given by (11) can be generalised for two subsystems, one is designed for the position Σ_P and the other is for the attitude Σ_A in which the translational and rotational dynamics are considered as disturbed non-linear second-order systems. The following subsystems will be used in the control design:

$$\Sigma_P: \begin{cases} \dot{x}_1 = x_2 \\ \dot{x}_2 = f_1(x) + g_1(x)T, \end{cases} \tag{14}$$

$$\Sigma_A: \begin{cases} \dot{x}_3 = x_4 \\ \dot{x}_4 = f_2(x) + g_2(x)U, \end{cases} \tag{15}$$

https://doi.org/10.1017/aer.2022.72 Published online by Cambridge University Press

with $f_1 = \begin{bmatrix} f_x & f_y & f_z \end{bmatrix}^T$ is written as:

$$f_1(x) = f_{01} + d_1, \tag{16}$$

and $f_2 = \begin{bmatrix} f_\phi & f_\theta & f_\psi \end{bmatrix}^T$ is written as:

$$f_2(x) = f_{02} + d_2, \tag{17}$$

where $x_\xi = \begin{bmatrix} x_1 & x_2 \end{bmatrix} \in \mathbb{R}^{3\times 2}$ is the vector of states for position, $x_1 = \begin{bmatrix} x & y & z \end{bmatrix}^T \in \mathbb{R}^3$, $x_2 = \begin{bmatrix} \dot{x} & \dot{y} & \dot{z} \end{bmatrix}^T \in \mathbb{R}^3$, $T = \begin{bmatrix} U_x & U_y & U_1 \end{bmatrix}^T$ is the vector of control inputs and the bounded disturbance $d_1 = \begin{bmatrix} d_x & d_y & d_z \end{bmatrix} \in \mathbb{R}^3$

$x_\eta = \begin{bmatrix} x_3 & x_4 \end{bmatrix} \in \mathbb{R}^{3\times 2}$ is the vector of states for attitude, $x_3 = \begin{bmatrix} \phi & \theta & \psi \end{bmatrix}^T \in \mathbb{R}^3$ and $x_4 = \begin{bmatrix} \dot{\phi} & \dot{\theta} & \dot{\psi} \end{bmatrix}^T \in \mathbb{R}^3$, $U = \begin{bmatrix} U_2 & U_3 & U_4 \end{bmatrix}^T$ is the vector of control inputs and the bounded disturbance $d_2 = \begin{bmatrix} d_\phi & d_\theta & d_\psi \end{bmatrix} \in \mathbb{R}^3$. $g_1(x)$ and $g_2(x)$) belong to $\mathbb{R}^{3\times 3}_*$. The functions f_{01} and f_{02} represent the known terms of $f_1(x)$ and $f_2(x)$ respectively.

2.3 Control objective

The main objective is to design a control laws T and U such that the variable $(x_\xi(t), x_\eta(t))$ track robustly the desired signals $(x_{\xi d}(t), x_{\eta d}(t))$, i.e. to render the tracking error

$$\begin{pmatrix} \varrho_1(t) \\ \varrho_3(t) \end{pmatrix} \equiv \begin{pmatrix} x_\xi(t) - x_{\xi d}(t) \\ x_\eta(t) - x_{\eta d}(t) \end{pmatrix} \equiv \begin{pmatrix} 0 \\ 0 \end{pmatrix} \text{ in finite time } t_R.$$

3.0 Adopted control architecture

The dynamics of the unconventional quadrotor are strongly non-linear and relatively complex because of the difficulty of modeling aerodynamic forces (aerodynamic coefficient, air density, and apparent surface) and the uncertainty of the physical constants of the drone. Robust control techniques are used to ensure the stability of the vehicle in the presence of external disturbances, despite the complexity of the aerodynamic forces and the impossibility of directly measuring the wind speed. These unknown terms are considered disturbances.

3.1 Backstepping design

The backstepping control technique performs successive relations to make the looped system equivalent to stable cascaded first-order sub-systems in the Lyapunov sense, thus building a control law and a stabilising Lyapunov function. This method begins with the definition of the Lyapunov function. The principle is to construct at each step a gap between the current state of the system and a virtual controller that would guarantee the negativity of the derivative of the Lyapunov function. At the end of each step, the Lyapunov function compensates this gap, to ensure the convergence to zero. The process ends when the real control of the system appears, guaranteeing the convergence of the real states to the desired states.

The control laws by backstepping combined with the ST algorithm are designed as:

$$T = g_1^{-1}(x)\,(-f_{01}(x) + \dot{\upsilon}_1 + \upsilon_2), \tag{18}$$

with

$$\begin{cases} \upsilon_1 = \dot{x}_{1d} - \kappa_1\, \varrho_1 \\ \upsilon_2 = -\lambda_1\, \mathfrak{Sig}^{\frac{1}{2}}(\varrho_2) - \lambda_2\, \mathfrak{Int}(\varrho_2), \end{cases} \tag{19}$$

$$U = g_2^{-1}(x)\,(-f_{02}(x) + \dot{\upsilon}_3 + \upsilon_4), \tag{20}$$

https://doi.org/10.1017/aer.2022.72 Published online by Cambridge University Press

with

$$\begin{cases} \upsilon_3 = \dot{x}_{3d} - \kappa_2\, \varrho_3 \\ \upsilon_4 = -\lambda_3\, \mathfrak{Sig}^{\frac{1}{2}}(\varrho_4) - \lambda_4\, \mathfrak{Int}(\varrho_4), \end{cases} \tag{21}$$

where $\left(\kappa_1 = \text{diag}\left[\kappa_x \quad \kappa_y \quad \kappa_z\right], \kappa_2 = \text{diag}\left[\kappa_\phi \quad \kappa_\theta \quad \kappa_\psi\right]\right) \in \mathbb{R}_{+*}^{3\times 3}$
and $\lambda_1 = \text{diag}\left[\lambda_{1x} \quad \lambda_{1y} \quad \lambda_{1z}\right], \lambda_2 = \text{diag}\left[\lambda_{2x} \quad \lambda_{2y} \quad \lambda_{2z}\right],$
$\lambda_3 = \text{diag}\left[\lambda_{1\phi} \quad \lambda_{1\theta} \quad \lambda_{1\psi}\right], \lambda_4 = \text{diag}\left[\lambda_{2\phi} \quad \lambda_{2\theta} \quad \lambda_{2\psi}\right]$

Theorem 1. *Considering the disturbed systems (14) and (15) with bounded condition (25) and the applied control inputs (18) and (20). The state variables (x_ξ, x_η) of systems (14) and (15), respectively, can track exactly the desired references ($x_{\xi d}$, $x_{\eta d}$) and converge in a finite time t_R.*

The following Lemma is used for the stability analysis

Lemma 1. *[33, 34] Considering the continuous system*

$$\dot{x} = f(x), \quad f(0) = 0, \quad x \in \mathbb{R}^n. \tag{22}$$

We suppose that there is a continuous positive definite function V: $\mathbb{R}^n \to \mathbb{R}^+$, a real number $\gamma > 0$, $0 < \alpha < 1$ and an open $U \subseteq \mathbb{R}^n$ in the neighbourhood of the origin so that the following inequalities are satisfied:

$$\dot{V}(x) + \gamma\, V^\alpha(x) \leq 0, \quad x \in V \setminus \{0\}. \tag{23}$$

Then, the origin of the system (22) is a stable equilibrium in finite time. If $U = \mathbb{R}^n$, the origin is a globally stable equilibrium in finite time.

Moreover, the settling time is given by:

$$t_R \leq \frac{1}{\gamma(1-\alpha)} V^{1-\alpha}. \tag{24}$$

Assumption 1. *The perturbation terms d_1 and d_2 are assumed to be bounded, such that:*

$$\| \dot{d}_1 \| < h_{1max} \qquad and \qquad \| \dot{d}_2 \| < h_{2max}, \tag{25}$$

where h_{1max} and h_{2max} are strictly positive constants supposed to be known.

Proof. *We follow these steps to prove the previous theorem:* □

3.1.1 First step

Consider system (14)

Let us define the tracking error ϱ_1:

$$\varrho_1 = x_1 - x_{1d}. \tag{26}$$

The first Lyapunov candidate function $\mathcal{L}_1$, associated with ϱ_1 is given by:

$$\mathcal{L}_1 = \frac{1}{2} \varrho_1^T \varrho_1. \tag{27}$$

Its temporal derivative:

$$\dot{\mathcal{L}}_1 = \varrho_1^T\, \dot{\varrho}_1 = \varrho_1^T (\dot{x}_1 - \dot{x}_{1d}) = \varrho_1^T\, (\dot{x}_1 - \upsilon_1) + \varrho_1^T\, (\upsilon_1 - \dot{x}_{1d})\,. \tag{28}$$

The term $(\dot{x}_{1d})$ represents the velocity set point and υ_1 is the stabilising controller of ϱ_1.

$$\upsilon_1 = \dot{x}_{1d} - \kappa_1\, \varrho_1. \tag{29}$$

Replacing (29) in (28), we obtain:

$$\dot{\mathcal{L}}_1 = -\varrho_1^T\, \kappa_1\, \varrho_1 + \varrho_1^T (\dot{x}_1 - \upsilon_1). \tag{30}$$

https://doi.org/10.1017/aer.2022.72 Published online by Cambridge University Press

3.1.2 Second step

The error ϱ_2 is defined as the difference between the real velocity and the virtual velocity control. The convergence of ϱ_2 will naturally lead to the convergence of ϱ_1, since the velocity will tend towards the virtual velocity and the derivative of $\mathcal{L}_1$ will be strictly negative.

Let us define the error ϱ_2:

$$\varrho_2 = \dot{x}_1 - \upsilon_1. \tag{31}$$

We define the second Lyapunov candidate function $\mathcal{L}_2$, associated with ϱ_2.

$$\mathcal{L}_2 = \frac{1}{2}\,\varrho_2^T \varrho_2. \tag{32}$$

The derivative of the Lyapunov function is given by:

$$\dot{\mathcal{L}}_2 = \varrho_2^T\,\dot{\varrho}_2 = \varrho_2^T\ \left(f(x) + g(x)\,T - \dot{\upsilon}_1\right). \tag{33}$$

The control law is given by:

$$T = g^{-1}(x)\ \left(-f_0(x) + \dot{\upsilon}_1 + \upsilon_2\right). \tag{34}$$

Replacing (34) in (33), we obtain

$$\dot{\mathcal{L}}_2 = \varrho_2^T\ \left(d_1 + \upsilon_2\right). \tag{35}$$

We take υ_2 as

$$\upsilon_2 = -\lambda_1\,\mathfrak{Sig}^{\frac{1}{2}}(\varrho_2) - \lambda_2\,\mathfrak{Int}(\varrho_2). \tag{36}$$

We replace (36) in (35), we find

$$\dot{\mathcal{L}}_2 = \varrho_2^T\left(-\lambda_1\,\mathfrak{Sig}^{\frac{1}{2}}(\varrho_2) - \lambda_2\,\mathfrak{Int}(\varrho_2) + d_1\right). \tag{37}$$

We make the following change of variable

$$z = \begin{bmatrix} z_1 & z_2 \end{bmatrix}^T, \tag{38}$$

$$\begin{cases} z_1 = \varrho_2 \\ z_2 = -\lambda_2\,\mathfrak{Int}(\varrho_2) + d_1 \end{cases}. \tag{39}$$

Which implies

$$\begin{cases} \dot{z}_1 = -\lambda_1\,\mathfrak{Sig}^{\frac{1}{2}}(z_1) + z_2 \\ \dot{z}_2 = -\lambda_2\,\dot{\mathfrak{Int}}(z_1) + \dot{d}_1 \end{cases}. \tag{40}$$

The convergence of z_1 and z_2 to zero ensures the convergence of ϱ_2 and $\dot{\varrho}_2$ to zero.

We choose now the following Lyapunov function to analyse the stability:

$$V(z) = v^T P\, v. \tag{41}$$

The vector v and the symmetric matrix $P \in \mathbb{R}^{2\times 2}$ are given by:

$$v = \begin{bmatrix} \mathfrak{Sig}^{\frac{1}{2}}(z_1) & z_2 \end{bmatrix}^T \quad \text{and} \quad P = \frac{1}{2}\begin{bmatrix} 4\lambda_2 + \lambda_1^2 & -\lambda_1 \\ -\lambda_1 & 2 \end{bmatrix}, \tag{42}$$

this function is defined positive if λ_2 is defined positive.

$$\delta_{min}(P)\|v\|^2 \ \leq\ V(z)\ \leq\ \delta_{max}(P)\|v\|^2, \tag{43}$$

https://doi.org/10.1017/aer.2022.72 Published online by Cambridge University Press

where v is given by:

$$\|v\|^2 = \|z_1\| + z_2^2, \tag{44}$$

$\delta_{min}(P)$ and $\delta_{max}(P)$ are respectively the minimal and maximal eigenvalues of P.

Knowing that $\| \dot{d}_1 \| \leq h_{1max}$ (see Assumption 1), the temporal derivative of the candidate Lyapunov function verify that:

$$\dot{V} \leq -\frac{1}{\|z_1\|^{\frac{1}{2}}} \delta_{min}(Q) \|v\|^2 + h_{1max} \|\xi\| \|v\|, \tag{45}$$

where

$$Q = \frac{\lambda_1}{2} \begin{bmatrix} 2\lambda_2 + \lambda_1^2 & -\lambda_1 \\ -\lambda_1 & 1 \end{bmatrix} \quad ; \quad \xi = \begin{bmatrix} -\lambda_1 & 2 \end{bmatrix}. \tag{46}$$

Using (44), we can deduce that

$$\frac{1}{\|z_1\|^{\frac{1}{2}}} \geq \frac{1}{\|v\|}. \tag{47}$$

We find

$$\dot{V} \leq (-\delta_{min}(Q) + h_{1max}\|\xi\|) \|v\|. \tag{48}$$

Using (43), we can see that:

$$\frac{V}{\delta_{max}(P)} \leq \|v\|^2 \leq \frac{V}{\delta_{min}(P)}. \tag{49}$$

We find

$$\dot{V} \leq -(\delta_{min}(Q) - h_{1max}\|\xi\|) \frac{V^{\frac{1}{2}}}{\sqrt{\delta_{max}(P)}}. \tag{50}$$

To conclude on the negativity of $\dot{V}(z)$, it is necessary that:

$$\delta_{min}(Q) \geq h_{1max}\|\xi\|. \tag{51}$$

The matrix Q will be defined positive with a minimal eigenvalue $\delta_{min}(Q) \geq h_{1max}||\xi||$, λ_1 defined positive and $h_{1max} > 0$, hence:

$$\lambda_2 \geq \frac{2\, h_{1max}^2 \|\xi\|^2}{\lambda_1^2}. \tag{52}$$

Therefore, we get

$$\dot{V} \leq -\gamma\, V^{\frac{1}{2}}. \tag{53}$$

with

$$\gamma = \frac{\delta_{min}(Q) - h_{1max}\|\xi\|}{\sqrt{\delta_{max}(P)}}. \tag{54}$$

The solution is

$$\int_0^{t_R} \frac{dV}{V^{\frac{1}{2}}} \leq -\gamma \int_0^{t_R} dt \Longrightarrow t_R = \frac{2V^{\frac{1}{2}}z(0)}{\gamma}. \tag{55}$$

So, we have demonstrated the stability in finite time. i.e. z_1 and z_2 tend to zero in a finite time.

$$z_2 = 0 \Longrightarrow \quad d_1 = \lambda_2\, \mathfrak{Int}(z_1), \tag{56}$$

where $\lambda_2\, \mathfrak{Int}(z_1)$ represents the perturbation estimation term.

https://doi.org/10.1017/aer.2022.72 Published online by Cambridge University Press

As soon as $z_1 = z_2 = 0 \in \mathbb{R}_3$ and according to Equation (56), then:

$$\Longrightarrow \dot{\mathcal{L}}_2 = \varrho_2^T \left(-\lambda_1 \, \mathfrak{Sig}^{\frac{1}{2}}(\varrho_2)\right)$$

$$\Longrightarrow \dot{\mathcal{L}}_2 = -\sum_{i=1}^{3} \lambda_{1i} \mid \varrho_{2i} \mid\mid \varrho_{2i} \mid^{\frac{1}{2}}$$

$$\Longrightarrow \dot{\mathcal{L}}_2 = -\sum_{i=1}^{3} \lambda_{1i} \mid \varrho_{2i} \mid^{\frac{3}{2}}, \tag{57}$$

we define $\tilde{\lambda}_1 = min\{\lambda_{11}, \lambda_{12}, \lambda_{13}\}$, we get

$$\Longrightarrow \dot{\mathcal{L}}_2 \leq -\tilde{\lambda}_1 \sum_{i=1}^{3} \mid \varrho_{2i} \mid^{\frac{3}{2}}$$

$$\Longrightarrow \dot{\mathcal{L}}_2 \leq -\tilde{\lambda}_1 \sum_{i=1}^{3} \left(\frac{1}{2} 2 \mid \varrho_{2i} \mid^{\frac{3}{2}}\right)$$

$$\Longrightarrow \dot{\mathcal{L}}_2 \leq -\tilde{\lambda}_1 2^{\frac{3}{4}} \sum_{i=1}^{3} \left(\frac{1}{2} \mid \varrho_{2i} \mid^{\frac{3}{2}}\right). \tag{58}$$

Let $\tilde{\kappa}_1 = 2^{\frac{3}{4}} \tilde{\lambda}_1$

$$\Longrightarrow \dot{\mathcal{L}}_2 \leq -\tilde{\kappa}_1 \mathcal{L}_2^{\frac{3}{4}}$$

$$\Longrightarrow \dot{\mathcal{L}}_2 \leq -\tilde{\kappa}_1 \mathcal{L}_2^{\alpha}, \tag{59}$$

with $\alpha = \frac{3}{4} \in [0, 1]$

According to Lemma 1, $\mathcal{L}_2$ is stable, so the error $\varrho_2 \to 0$.

This implies that $\dot{\mathcal{L}}_1 = -\kappa_1 \parallel \varrho_1 \parallel^2$ is stable. Then, the error $\varrho_1 \to 0$.

Desired Euler angles

The unconventional quadrotor can be separated into two connected subsystems, based on the hierarchical backstepping. According to (13), we can calculate the desired Euler angles ϕ_d and θ_d, which will introduce the next error variable:

$$\begin{cases} \phi_d = \sin^{-1}\left(s\psi_d U_x - c\psi_d U_y\right) \\ \theta_d = \sin^{-1}\left(\dfrac{c\psi_d U_x + s\psi_d U_y}{c\phi_d}\right) \end{cases}. \tag{60}$$

3.1.3 Third step

Consider system (15), a new error variable is defined as:

$$\varrho_3 = x_3 - x_{3d}. \tag{61}$$

Consider the Lyapunov candidate function $\mathcal{L}_3$, associated with the error ϱ_3:

$$\mathcal{L}_3 = \frac{1}{2} \varrho_3^T \varrho_3. \tag{62}$$

Its derivative with respect to time yields:

$$\dot{\mathcal{L}}_3 = \varrho_3^T \, \dot{\varrho}_3 = \varrho_3^T (\dot{x}_3 - \dot{x}_{3d}) = \varrho_3^T (\dot{x}_3 - \upsilon_3) + \varrho_3^T (\upsilon_3 - \dot{x}_{3d}). \tag{63}$$

https://doi.org/10.1017/aer.2022.72 Published online by Cambridge University Press

The term $(\dot{x}_{3d})$ represents the velocity set point and υ_3 is the stabilising controller of ϱ_3.

$$\upsilon_3 = \dot{x}_{3d} - \kappa_2\, \varrho_3. \tag{64}$$

Replacing (64) in (63), we obtain:

$$\dot{\mathcal{L}}_3 = -\varrho_3^T\, \kappa_2\, \varrho_3 + \varrho_3^T(\dot{x}_3 - \upsilon_3), \tag{65}$$

the second term will be eliminated in the next step.

3.1.4 Fourth step

Consider the second term $\varrho_3(\dot{x}_3 - \upsilon_3)$ to continue the process of backstepping. The error ϱ_4 is defined as the difference between the real velocity and the virtual velocity control. The convergence of ϱ_4 will naturally lead to the convergence of ϱ_3, since the velocity will tend towards the virtual velocity and the derivative of $\mathcal{L}_3$ will be strictly negative.

Let define the error ϱ_4:

$$\varrho_4 = \dot{x}_3 - \upsilon_3. \tag{66}$$

The Lyapunov candidate function $\mathcal{L}_4$ associated with ϱ_4 is defined as:

$$\mathcal{L}_4 = \frac{1}{2}\, \varrho_4^T \varrho_4. \tag{67}$$

Its temporel derivative is given by:

$$\dot{\mathcal{L}}_4 = \varrho_4^T\, \dot{\varrho}_4 = \varrho_4^T\, (f(x) + g(x)\, U - \dot{\upsilon}_3). \tag{68}$$

The controller is given by:

$$U = g^{-1}(x)\, (-f_0(x) + \dot{\upsilon}_3 + \upsilon_4). \tag{69}$$

Replacing (69) in (68), we obtain

$$\dot{\mathcal{L}}_4 = \varrho_4^T\, (d_2 + \upsilon_4). \tag{70}$$

We take υ_4 as

$$\upsilon_2 = -\lambda_3\, \mathfrak{Sig}^{\frac{1}{2}}(\varrho_4) - \lambda_4\, \mathfrak{Int}(\varrho_4). \tag{71}$$

We replace (71) in (70), we find

$$\dot{\mathcal{L}}_4 = \varrho_4^T \left(-\lambda_3\, \mathfrak{Sig}^{\frac{1}{2}}(\varrho_4) - \lambda_4\, \mathfrak{Int}(\varrho_4) + d_2\right). \tag{72}$$

Consider the following change of variable

$$\bar{z} = \begin{bmatrix} z_3 & z_4 \end{bmatrix}^T, \tag{73}$$

$$\begin{cases} z_3 = \varrho_4 \\ z_4 = -\lambda_4\, \mathfrak{Int}(\varrho_4) + d_2 \end{cases}. \tag{74}$$

Which implies

$$\begin{cases} \dot{z}_1 = -\lambda_3\, \mathfrak{Sig}^{\frac{1}{2}}(z_3) + z_4 \\ \dot{z}_2 = -\lambda_4\, \dot{\mathfrak{Int}}(z_3) + \dot{d}_2 \end{cases}. \tag{75}$$

The convergence of z_3 and z_4 to zero ensures the convergence of ϱ_4 and $\dot{\varrho}_4$ to zero. Therefore, the disturbance d_2 will be estimated in finite time.

https://doi.org/10.1017/aer.2022.72 Published online by Cambridge University Press

As soon as z_3=z_4=0 and the disturbance is estimated, then:

$$\Longrightarrow \dot{\mathcal{L}}_4 \leq -\tilde{\kappa}_2 \mathcal{L}_4^{\alpha}, \tag{76}$$

where $\alpha = \frac{3}{4}$, $\tilde{\kappa}_2 = 2^{\frac{3}{4}}\tilde{\lambda}_3$ and $\tilde{\lambda}_3 = min\{\lambda_{31}, \lambda_{32}, \lambda_{33}\}$

According to Lemma 1, $\mathcal{L}_4$ is stable $\Rightarrow$ the error $\varrho_4 \to 0$.

which implies that $\dot{\mathcal{L}}_3 = -\kappa_2 \parallel \varrho_3 \parallel^2$ is stable. Then, the error $\varrho_3 \to 0$

3.2 Control architecture

Hierarchical control is known in aeronautics as guidance and piloting control. The system is decomposed into two cascaded subsystems: one for translation corresponding to the slow dynamics called the high level (outer loop) and the other for rotation corresponding to the fast dynamics called the low level (inner loop) (see Fig. 4).

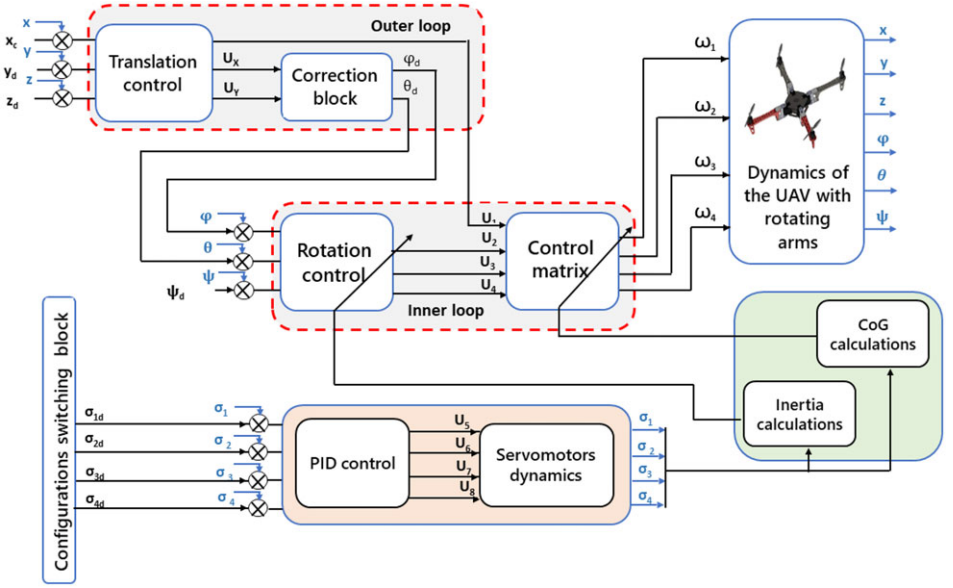

Figure 4. *Control architecture.*

The reference trajectories (x_d, y_d, z_d and ψ_d) are generated by the guidance system block. U_1 controls the attitude while the two other translation variables x and y are controlled indirectly by controlling the two rotation angles (ϕ and θ) with the virtual controllers U_x and U_y. The correction block will generate the desired roll and pitch angles. The foldable drone is controlled by the velocity of the motors. These velocities are obtained from the control matrix. The CoG and the inertia matrix are instantly calculated according to the variation of the angles σ_i. The different configurations of the quadrotor are generated by the switching block.

The main difficulty of this control structure is to demonstrate the stability of the global system in a closed loop and to guarantee good performance as well as robust behaviour towards disturbances. Servomotors are controlled by a classical PID to turn the arms, where:

$$U_s = k_p e_{\sigma_i}(t) + k_I \int e_{\sigma_i}(t)dt + k_D \dot{e}_{\sigma_i}(t), \tag{77}$$

with $e_{\sigma_i}(t)$ is the tracking error. k_p, k_I and k_D are the controller's gains.

https://doi.org/10.1017/aer.2022.72 Published online by Cambridge University Press

The studied quadrotor is controlled by a backstepping controller with a correction term based on the super-twisting algorithm, which is designed to follow the desired trajectory (x_d, y_d, z_d) and the angle ψ_d in the presence of disturbances.

3.3 Control inputs

Applying the control laws (34) and (69) on the systems (14) and (15) respectively, we obtain the final control inputs as:

Altitude control (z)

$$\begin{cases} \varrho_{11} = z - z_d \\ \varrho_{21} = \dot{z} - \upsilon_{11} \\ \upsilon_{11} = \dot{z}_d - \kappa_z \, \varrho_{11} \\ \upsilon_{21} = -\lambda_{1z} \, |\varrho_{21}|^{\frac{1}{2}} \, \text{sign}(\varrho_{21}) - \lambda_{2z} \int \text{sign}(\varrho_{21}(z)) dz \end{cases}$$

$$U_1 = \frac{1}{g_z(x)} \left(-f_z(x) + \dot{\upsilon}_{11} + \upsilon_{21}\right). \tag{78}$$

Roll control (ϕ)

$$\begin{cases} \varrho_{12} = \phi - \phi_d \\ \varrho_{22} = \dot{\phi} - \upsilon_{12} \\ \upsilon_{12} = \dot{\phi}_d - \kappa_\phi \, \varrho_{12} \\ \upsilon_{22} = -\lambda_{1\phi} \, |\varrho_{22}|^{\frac{1}{2}} \, \text{sign}(\varrho_{22}) - \lambda_{2\phi} \int \text{sign}(\varrho_{22})(z) dz \end{cases}$$

$$U_2 = \frac{1}{g_\phi(x)} \left(-f_\phi(x) + \dot{\upsilon}_{12} + \upsilon_{22}\right). \tag{79}$$

Pitch control (θ)

$$\begin{cases} \varrho_{13} = \theta - \theta_d \\ \varrho_{23} = \dot{\theta} - \upsilon_{13} \\ \upsilon_{13} = \dot{\theta}_d - \kappa_\theta \, \varrho_{13} \\ \upsilon_{23} = -\lambda_{1\theta} \, |\varrho_{23}|^{\frac{1}{2}} \, \text{sign}(\varrho_{23}) - \lambda_{2\theta} \int \text{sign}(\varrho_{23}(z)) dz \end{cases}$$

$$U_3 = \frac{1}{g_\theta(x)} \left(-f_\theta(x) + \dot{\upsilon}_{13} + \upsilon_{23}\right). \tag{80}$$

Yaw control (ψ)

$$\begin{cases} \varrho_{14} = \psi - \psi_d \\ \varrho_{24} = \dot{\psi} - \upsilon_{14} \\ \upsilon_{14} = \dot{\psi}_d - \kappa_\psi \, \varrho_{14} \\ \upsilon_{24} = -\lambda_{1\psi} \, |\varrho_{24}|^{\frac{1}{2}} \, \text{sign}(\varrho_{24}) - \lambda_{2\psi} \int \text{sign}(\varrho_{24}(z)) dz \end{cases}$$

$$U_4 = \frac{1}{g_\psi(x)} \left(-f_\psi(x) + \dot{\upsilon}_{14} + \upsilon_{24}\right). \tag{81}$$

https://doi.org/10.1017/aer.2022.72 Published online by Cambridge University Press

Virtual controllers
Control of (x)

$$\begin{cases} \varrho_{1x} = x - x_d \\ \varrho_{2x} = \dot{x} - \nu_{1x} \\ \upsilon_{1x} = \dot{x}_d - \kappa_x \varrho_{1x} \\ \upsilon_{2x} = -\lambda_{1x} |\varrho_{2x}|^{\frac{1}{2}} \operatorname{sign}(\varrho_{2x}) - \lambda_{2x} \int \operatorname{sign}(\varrho_{2x}(z))dz \end{cases}$$

$$U_x = \frac{m}{U_1}(\dot{\upsilon}_{1x} + \upsilon_{2x}). \tag{82}$$

Control of (y)

$$\begin{cases} \varrho_{1y} = y - y_d \\ \varrho_{2y} = \dot{y} - \nu_{1y} \\ \upsilon_{1y} = \dot{y}_d - \kappa_y \varrho_{1y} \\ \upsilon_{2y} = -\lambda_{1y} |\varrho_{2y}|^{\frac{1}{2}} \operatorname{sign}(\varrho_{2y}) - \lambda_{2y} \int \operatorname{sign}(\varrho_{2y}(z))dz \end{cases}$$

$$U_y = \frac{m}{U_1}(\dot{\upsilon}_{1y} + \upsilon_{2y}). \tag{83}$$

4.0 Simulation results

In this section, we will present a series of simulations of two flight scenarios resulting from the application of the backstepping control previously seen on our drone to test the efficiency and robustness of the tracking problem.

To validate the efficiency of the proposed control, a qualitative comparison with a classical backstepping controller has been made in the presence of external disturbances. The ordinary backstepping control law applied to a reconfigurable UAV is detailed in [4].

We performed the simulations under MATLAB/Simulink. The numerical values of the main physical parameters of the quadrotor are provided in Table 2.

Table 2. *Parameters of the unconventional quadrotor*

Parameters	Value	Unit
Arm length d	0.21	m
Width and length of the central body a	0.075	m
Total mass m	1.100	kg
Gravity constant g	9.81	m/s^2
Rotor inertia J_r	$2.8385e-5$	kg/m^2

The servomotors are controlled by a PID, the parameters of this latter are given in Table 3 as:

Table 3. *Parameters of PID controller.*

Parameters	Value
k_p	33.06079
k_i	10
k_d	0.2

https://doi.org/10.1017/aer.2022.72 Published online by Cambridge University Press

Table 4. *Parameters of the controller.*

Parameters	Value
κ_z	1
κ_x, κ_y	0.25
κ_ϕ, κ_θ	0.3
κ_ψ	8000
λ_{1z}	2
λ_{1x}, λ_{1y}, $\lambda_{1\phi}$, $\lambda_{1\theta}$	3
$\lambda_{1\psi}$	40
λ_{2z}	0.1
λ_{2x}, λ_{2y}, $\lambda_{2\phi}$, $\lambda_{2\theta}$	0.2
$\lambda_{2\psi}$	0.01

We note that the simulations were done in the presence of external disturbances that are noted as $d_1 = 0.5\text{N.kg}^{-1}$ for translation and $d_2 = 0.01\text{N.(kg.m)}^{-1}$ for rotation.

The main controller parameters are summarised in Table 4.

4.1 Scenario 1

In this scenario, we make a square trajectory where the foldable drone changes its configuration during the flight. Simulation results are presented in Figs 5 to 11. Figure 5 represents the absolute position of the quadrotor during its flight. The translation and attitude responses are displayed in Figs 6 and 7, while the control signals are illustrated in Fig. 10.

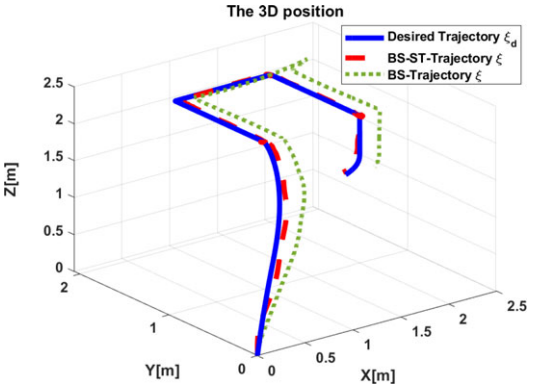

Figure 5. *Absolute position of the quadrotor under disturbances.*

According to Figs 6 and 7, the quadrotor follows the reference trajectories. It is observed in Figs 8 and 9 that the tracking error converges to zero due to the effectiveness of the proposed controller. Figure 10 shows the evolution of the control signals. We notice that U_2 and U_3 contain chattering. This is due to the discontinuous function sign in control laws, this switching in control excites the unmodeled dynamics, which leads to oscillations of the state vector. From Fig. 11, the servomotors' output follows the desired angles with some error in the descent and ascent, which is generated by the rotation of their arms.

https://doi.org/10.1017/aer.2022.72 Published online by Cambridge University Press

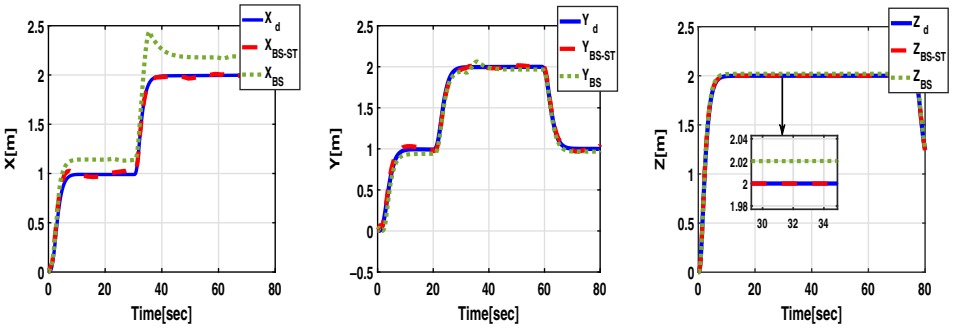

Figure 6. *Trajectory of positions.*

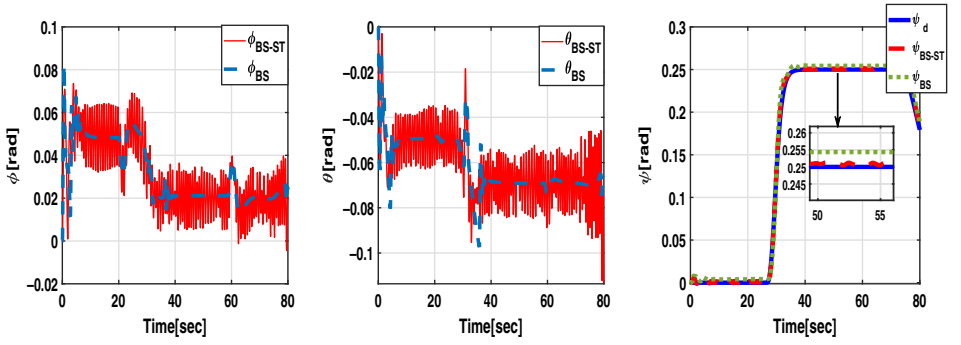

Figure 7. *Euler angles.*

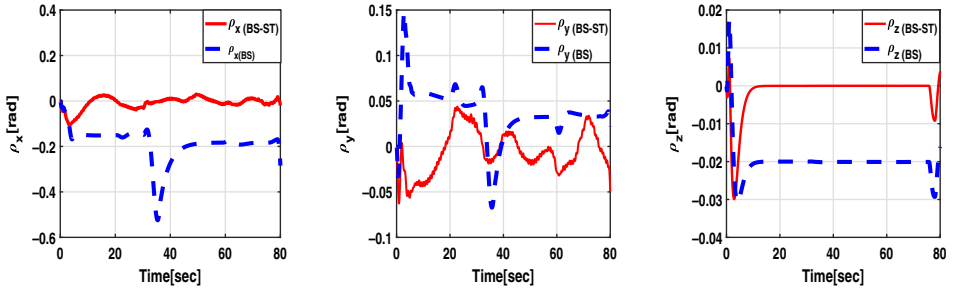

Figure 8. *Quadrotor tracking errors.*

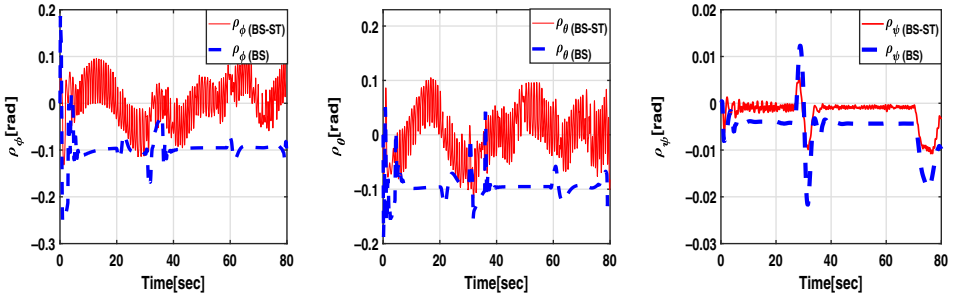

Figure 9. *Quadrotor attitude errors.*

https://doi.org/10.1017/aer.2022.72 Published online by Cambridge University Press

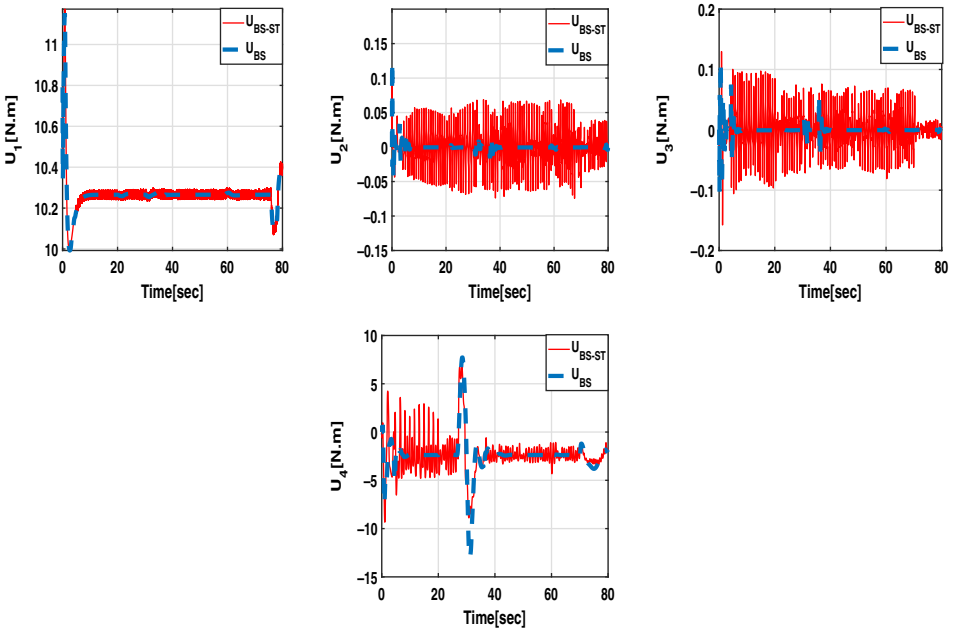

Figure 10. *Evolution of control signals.*

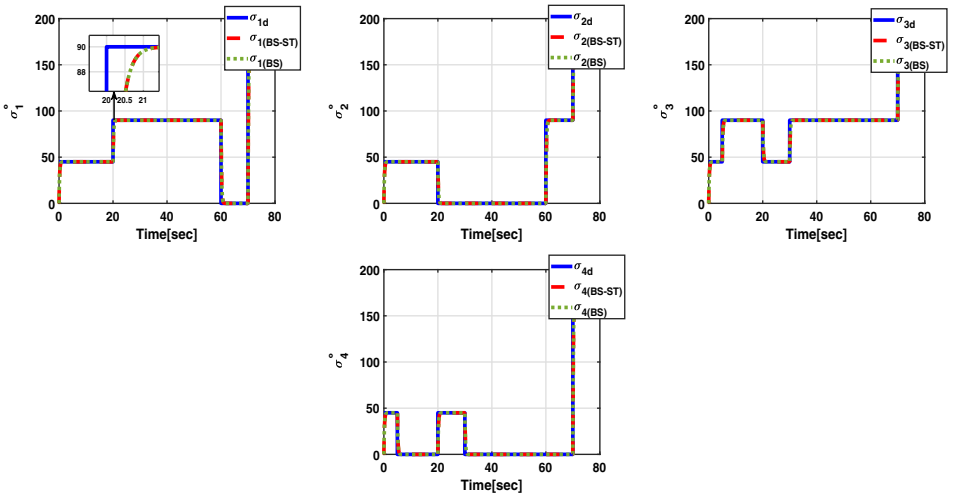

Figure 11. *Servomotors outputs.*

The efficiency of the proposed control method is illustrated in Figs 5 to 10 via the comparison between the results obtained using the proposed controller and the classical backstepping presented in [4] in the presence of external disturbances. In comparison to the classical backstepping controller provided, the simulation results clearly indicate better performance, quicker convergence, high precision tracking, and resilience.

In the light of these results, we have demonstrated the efficiency of this control approach to follow the desired trajectories and simulate them in the presence of disturbances.

https://doi.org/10.1017/aer.2022.72 Published online by Cambridge University Press

4.2 Scenario 2

In this scenario, we make a circular trajectory, which is more complex. The obtained results are displayed in Figs 12 to 17. Figure 12 shows the absolute position of the quadrotor during the flight in the circular trajectory. Figures 13 and 14 represent the evolution of the position and orientation of the vehicle. The actuator force controls are displayed in Fig. 17.

On the basis of these results, we can clearly see from Figs 12, 13 and 14 a good tracking of the desired trajectories. We can also see that the outputs of the system converge towards the setpoint trajectories quickly. We notice the presence of chattering in the evolution of the control signals due to the switching in control laws.

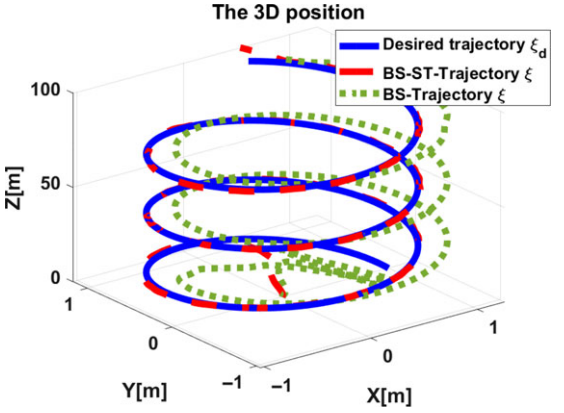

Figure 12. *Absolute position of the quadrotor under disturbances.*

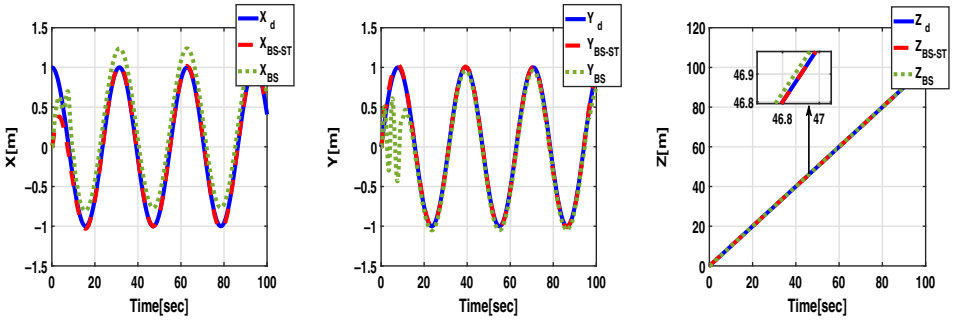

Figure 13. *Trajectory of positions.*

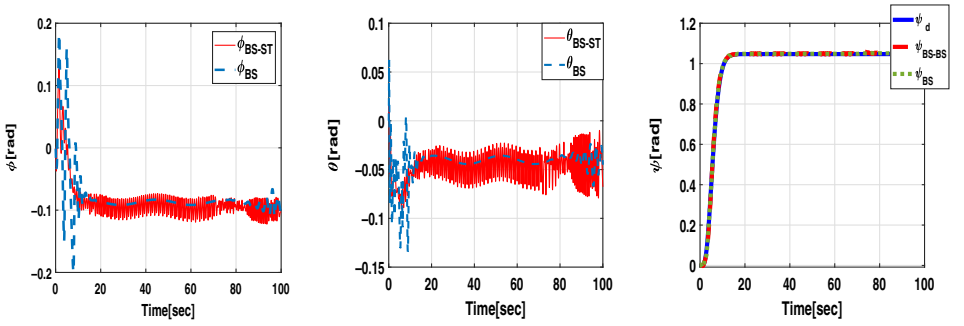

Figure 14. *Euler angles.*

https://doi.org/10.1017/aer.2022.72 Published online by Cambridge University Press

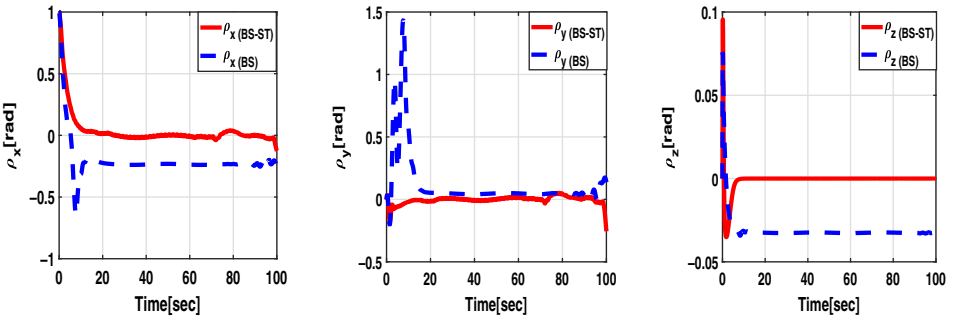

Figure 15. *Quadrotor tracking errors.*

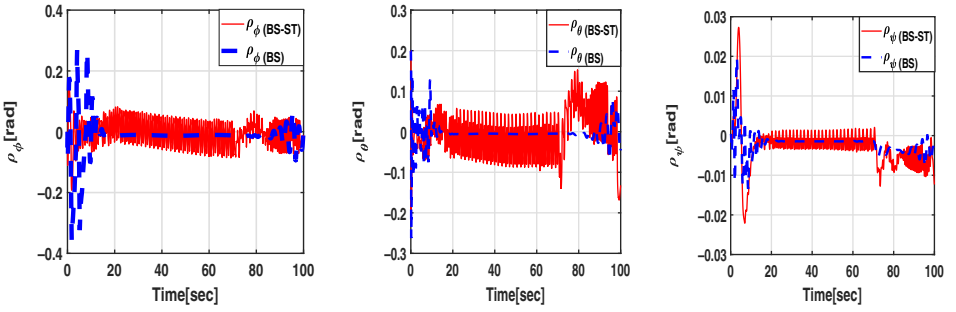

Figure 16. *Quadrotor attitude errors.*

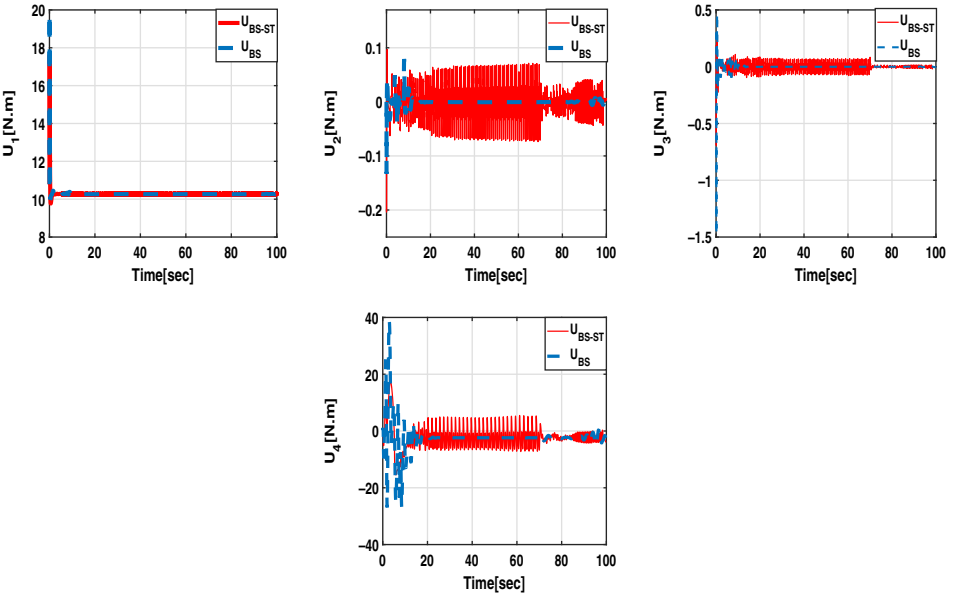

Figure 17. *Evolution of control signals.*

https://doi.org/10.1017/aer.2022.72 Published online by Cambridge University Press

The comparison between the results obtained using the proposed controller and the classical backstepping is illustrated in Figs 12 to 17 in the presence of external disturbances. When compared to the classical backstepping controller presented in Ref.(4), the simulation results clearly demonstrate satisfactory performance, faster convergence, high accuracy tracking and robustness.

Using the simulation results, we have demonstrated the efficiency of this control approach to follow the desired trajectories and to adapt to the change in the flight configuration. Furthermore, simulations have shown the robustness of the proposed control in the presence of disturbances. We interpret this by the introduction of the correction term based on the super-twisting algorithm.

To better clarify the comparison and strengthen our results, we have opted for a quantitative comparison with respect to the trajectory error and the control inputs.

The Mean Squared Error *MSE* and the Mean Squared Input *MSI* are calculated for N points as follows:

$$\begin{cases} MSE_{\text{position}} = \dfrac{1}{N}\left(\varrho_x^T\varrho_x + \varrho_y^T\varrho_y + \varrho_z^T\varrho_z\right) \\ MSE_{\text{attitude}} = \dfrac{1}{N}\left(\varrho_\phi^T\varrho_\phi + \varrho_\theta^T\varrho_\theta + \varrho_\psi^T\varrho_\psi\right) \\ MSI = \dfrac{1}{N}\left(U_1^TU_1 + U_2^TU_2 + U_3^TU_3 + U_4^TU_4\right) \end{cases} . \tag{84}$$

In addition to the results found previously, the comparison between the two control laws in terms of error and input shows the efficiency of our proposed controller, in which the calculated values of the controller based on the super-twisting algorithm are lower than the classical backstepping controller, and this is proven in both scenarios (see Tables 5 and 6). The two values, *MSE* and *MSI* are considered, respectively, as the tracking error and the energy consumed during the flight.

Table 5. *Quantitative comparison for the* 1^{st} *scenario*

	Proposed control	Classical backstepping control
MSE_{position}	0.0014	0.0409
MSE_{attitude}	0.0048	0.0210
MSI	115.5037	115.6780

Table 6. *Quantitative comparison for the* 2^{nd} *scenario*

	Proposed control	Classical backstepping control
MSE_{position}	0.0210	0.2109
MSE_{attitude}	0.0051	0.0101
MSI	130.3683	143.0445

5.0 Conclusion and future works

In this paper, we have examined the problem of flight path tracking of the unconventional quadrotor in the presence of disturbances. We have briefly presented the mathematical model of the studied UAV. This step is crucial to obtain simulation results as close as possible to those of the real system. Then, a robust control strategy is developed and applied to a model of our foldable drone. This control law is robust, non-linear, and based on the Lyapunov stability theorem. The backstepping control with a correction term based on the super-twisting algorithm ensures stability in finite time and cancels the

https://doi.org/10.1017/aer.2022.72 Published online by Cambridge University Press

effect of the perturbation. The simulation results have shown that the proposed controller is able to improve the control performance of the quadrotor with rotating arms subjected to external disturbances. To provide faster convergence, a better ability to reject disturbances and improve robustness level to uncertainties and disturbances in the model of the quadrotor, we propose, in future, to enhanced the proposed controller by adding finite-time disturbance observer.

References

[1] Derafa, L., Ouldali, A., Madani, T. and Benallegue, A. Non-linear control algorithm for the four rotors UAV attitude tracking problem, *Aeronaut. J.*, 2011, **115**, (1165), pp 175–185.

[2] Yuan, S., Wang, H. and Xie, L. Survey on localization systems and algorithms for unmanned systems, *Unmanned Syst.*, 2021, **9**, (2), pp 129–163.

[3] Mokhtari, M.R. and Cherki, B. A new robust control for minirotorcraft unmanned aerial vehicles, *ISA Trans.*, 2015, **56**, pp 86–101.

[4] Derrouaoui, S.H., Bouzid, Y., Guiatni, M., Kada, H., Dib, I. and Moudjari, N. Backstepping controller applied to a foldable quadrotor for 3d trajectory tracking, In *ICINCO*, pp 537–544, 2020.

[5] Desbiez, A., Expert, F., Boyron, M., Diperi, J., Viollet, S. and Ruffier, F. X-morf: A crash-separable quadrotor that morfs its x-geometry in flight, In 2017 *Workshop on Research, Education and Development of Unmanned Aerial Systems (RED-UAS)*, pp 222–227. IEEE, 2017.

[6] Derrouaoui, S.H., Bouzid, Y., Guiatni, M. and Belmouhoub, A. Trajectory tracking of a reconfigurable multirotor using optimal robust sliding mode controller, 2022.

[7] Falanga, D., Mueggler, E., Faessler, M. and Scaramuzza, D. Aggressive quadrotor flight through narrow gaps with onboard sensing and computing using active vision, In *International Conference on Robotics and Automation (ICRA)*, pp 5774–5781. IEEE, 2017.

[8] Mintchev, S. and Floreano, D. Adaptive morphology: A design principle for multimodal and multifunctional robots, *Robot. Automat. Mag.*, 2016, **23**, (3), pp 42–54.

[9] Floreano, D. and Wood, R.J. Science, technology and the future of small autonomous drones, *Nature*, 2015, **521**, (7553), pp 460–466.

[10] Caballero, A., Suarez, A., Real, F., Vega, V.M., Bejar, M., Rodriguez-Castaño, A. and Ollero, A. First experimental results on motion planning for transportation in aerial long-reach manipulators with two arms, In *International Conference on Intelligent Robots and Systems (IROS)*, pp 8471–8477. IEEE, 2018.

[11] Yilmaz, E., Zaki, H. and Unel, M. Nonlinear adaptive control of an aerial manipulation system, In *18th European Control Conference (ECC)*, pp 3916–3921. IEEE, 2019.

[12] Derrouaoui, S.H., Bouzid, Y., Guiatni, M., Dib, I. and Moudjari, N. Design and modeling of unconventional quadrotors, In *28th Mediterranean Conference on Control and Automation (MED)*, pp 721–726. IEEE, 2020.

[13] Kamil, Y., Hazry, D., Wan, K., Razlan, Z.M. and Shahriman, A.B. Design a new model of unmanned aerial vehicle quadrotor using the variation in the length of the arm, In *International Conference on Artificial Life and Robotics (ICAROB), Miyazaki, Japan*, pp 19–22, 2017.

[14] Hazry, D., Wan, K. and Razlan, Z.M. A novel val: Quadrotor control technique for trajectory tracking based on varying the arm's length, *ARPN J. Eng. Appl. Sci.*, 2016, **11**, (15), pp 9195–9204.

[15] Derrouaoui, S.H., Bouzid, Y., Guiatni, M. and Dib, I. A comprehensive review on reconfigurable drones: Classification, characteristics, design and control technologies, *Unmanned Syst.*, 2021, pp 1–27.

[16] Sheng, S. and Sun, C. Control and optimization of a variable-pitch quadrotor with minimum power consumption, *Energies*, 2016, **9**, (4), p 232.

[17] Muliadi, J. The analysis of unconventional aircraft flight dynamics model by linearizing its equation of motion as applied in BPPT's V-tail configuration UAV "Gagak", *In AIP Conference Proceedings*, p 020060. AIP Publishing LLC, 2016.

[18] Invernizzi, D., Giurato, M., Gattazzo, P. and Lovera, M. Full pose tracking for a tilt-arm quadrotor UAV, In *Control Technology and Applications (CCTA)*, pp 159–164. IEEE, 2018.

[19] Farrell, M., Jackson, J., Nielsen, J., Bidstrup, C. and McLain, T. Error-state LQR control of a multirotor UAV, In *International Conference on Unmanned Aircraft Systems (ICUAS)*, pp 704–711. IEEE, 2019.

[20] Hamadi, H., Lussier, B., Fantoni, I., Francis, C. and Shraim, H. Observer-based super twisting controller robust to wind perturbation for multirotor UAV. In *International Conference on Unmanned Aircraft Systems (ICUAS)*, pp 397–405. IEEE, 2019.

[21] Sartori, D., Quagliotti, F., Rutherford, M.J. and Valavanis, K.P. Design and development of a backstepping controller autopilot for fixed-wing uavs. *Aeronaut. J.*, 2021, **125**, (1294), pp 2087–2113.

[22] Gao, T.Y., Wang, D.D., Tao, F. and Ge, H.L. Control of small unconventional UAV based on an on-line adaptive ADRC system, *In Applied Mechanics and Materials*, pp 1206–1211. Trans Tech Publ, 2014.

[23] De Almeida, M.M. and Raffo, G.V. Nonlinear control of a Tiltrotor UAV for load transportation, *IFAC-PapersOnLine*, 2015, **48**, (19), pp 232–237.

[24] Andrade, R., Raffo, G.V. and Normey-Rico, J.E. Model predictive control of a tilt-rotor UAV for load transportation, In *European Control Conference (ECC)*, pp 2165–2170. IEEE, 2016.

https://doi.org/10.1017/aer.2022.72 Published online by Cambridge University Press

[25] Willis, J., Johnson, J. and Beard, R.W. State-dependent LQR control for a Tilt-rotor UAV, In *American Control Conference (ACC)*, pp 4175–4181. IEEE, 2020.
[26] Wallace, D.A. *Dynamics and control of a quadrotor with active geometric morphing*, PhD thesis, 2016.
[27] Barbaraci, G. Modeling and control of a quadrotor with variable geometry arms, *Unmanned Veh. Syst.*, 2015, **3**, (2), pp 35–57.
[28] Falanga, D., Kleber, K., Mintchev, S., Floreano, D. and Scaramuzza, D. The foldable drone: A morphing quadrotor that can squeeze and fly, *Robot. Automat. Lett.*, 2018, **4**, (2), pp 209–216.
[29] Tuna, T., Ovur, S.E., Gokbel, E. and Kumbasar, T. Folly: A self foldable and self deployable autonomous quadcopter, In 2018 *6th International Conference on Control Engineering & Information Technology (CEIT)*, pp 1–6. IEEE, 2018.
[30] Chanzy, Q. and Keane, A.J. Analysis and experimental validation of morphing uav wings, *Aeronaut. J.*, 2018, **122**, (1249), pp 390–408.
[31] Derrouaoui, S.H., Bouzid, Y. and Guiatni, M. Towards a new design with generic modeling and adaptive control of a transformable quadrotor, *Aeronaut. J.*, 2021, **125**, (1294), pp 1–31.
[32] Derrouaoui, S.H., Guiatni, M., Bouzid, Y., Dib, I. and Moudjari, N. Dynamic modeling of a transformable quadrotor, In *International Conference on Unmanned Aircraft Systems (ICUAS)*, pp 1714–1719. IEEE, 2020.
[33] Bhat, S.P. and Bernstein, D. Finite-time stability of continuous autonomous systems. *Cont. Optimiz.*, 2000, **38**, (3), pp 751–766.
[34] Bhat, S.P. and Bernstein, D. Continuous finite-time stabilization of the translational and rotational double integrators, *Automat. Cont.*, 1998, **43**, (5), pp 678–682.

Amina Belmouhoub received the engineering degree from the Higher School of Applied Sciences, Tlemcen, Algeria (in 2020) and the Master's degree in automatic from the same school (in 2020). She is currently pursuing Ph.D. degree in Automatic at the laboratory of Materials and Electronic Systems of Bordj Bou Arreridj University. Her research interests include nonlinear and robust control, energy optimisation, quadrotors, reconfigurable multirotors and mobile robots.

Slimane Medjmadj received the engineering and Magister degrees in Electrotechnics from the University of Ferhat Abbas, Setif, Algeria, in 1996 and 2005, respectively. He received Ph.D. degree from the same university in 2015. He is currently an associate professor of control engineering and automation systems and the head of the Electromechanical Engineering Department of the Faculty of Science and Technology at the University of Bordj Bou Arreridj, Algeria. His main research interests include advanced control techniques, diagnosis, and fault-tolerant control of industrial systems.

Yasser Bouzid received the engineering degree from the Ecole Militaire Polytechnique (EMP), Bordj-el-Bahri, Algiers, Algeria (in 2013) and the Master of Science (MSc) from the University of Paris XI, France (in 2015). He received Ph.D. degree in Automatic from Paris Saclay University in 2018. He is currently an assistant professor at the EMP and a member in the laboratory of Complex Systems Control and Simulators (CSCS). His research interests include nonlinear control, fault-tolerant control, observation and estimation, path planning, heuristic algorithms, unmanned aerial vehicles, mobile robots, multi-agent systems, soft robotics.

Saddam Hocine Derrouaoui received the engineering degree from the Ecole Supérieure Ali Chabati, Réghaia, Algiers, Algeria (in 2016) and the Master degree in systems guidance and automatic from the same school (in 2016). He is now pursuing doctorate in Automatic in the laboratory of Complex Systems Control and Simulators (CSCS) of the Ecole Militaire Polytechnique (EMP). His research interests include nonlinear control, unmanned aerial vehicles, transformable and reconfigurable drones, mobile robots and manipulator arms.

Mohamed Guiatni received the bachelor of engineering and Master of Science (MSc) degrees both from the Ecole Militaire Polytechnique (EMP), Bordj-el-Bahri, Algiers, Algeria and the PhD degree from the University of Evry, France in 2009. He is currently the head of the Complex Systems Control and Simulators Laboratory and full professor at the EMP. His research interests include haptic devices design and control, mechatronics, rehabilitation robotics, interactive simulation for military and medical applications, UAV design and control.

Cite this article: Belmouhoub A., Medjmadj S., Bouzid Y., Derrouaoui S.H. and Guiatni M. (2023). Enhanced back-stepping control for an unconventional quadrotor under external disturbances. *The Aeronautical Journal*, **127**, 627–650. https://doi.org/10.1017/aer.2022.72